Numerical investigation of Wind Environment and Summer Thermal Comfort around Elevated Walkways

Lan CHEN[1], Kuen Wai MA[1], Shicheng CAO[1], Cheuk Ming MAK[1*]

[1]Department of Building Environment and Energy Engineering, The Hong Kong Polytechnic University, Postdoctoral Fellow/Postdoctoral Fellow/ Research Assistant/ Professor
[2]Department of Mechanical Engineering, National Taipei University of Technology, Assisstant Professor

Abstract

As an effective way to enhance road safety and pedestrian walkability, elevated walkways have gained increasing popularity in high-density cities. Given the insufficient understanding of wind environment and thermal comfort around elevated walkways, this study systematically investigates pedestrian-level wind environment and summer thermal comfort around parallel and covered elevated walkways in ideal urban building groups using large eddy simulation (LES) and RayMan modeling. The impacts of street height-width-ratio (H/W) and walkway width (W_{ew}/W) on ground-level and walkway-level wind and thermal comfort are revealed. Results indicate that constructing an elevated walkway worsens the ground pedestrian-level wind environment and summer thermal comfort by lowering the mean wind velocity (v). However, elevated walkways provide a significantly lower walkway-level physiological equivalent temperature (PET) than the ground-level one, effectively improving thermal comfort and mitigating heat stress in summer. Besides, both ground-level and walkway-level PET increase first and then decrease with H/W, but they continually increase with W_{ew}/W. In contrast, ground-level and walkway-level v show opposite variation trends to PET regarding both H/W and W_{ew}/W.

Keywords: Pedestrian-level Wind, Thermal Comfort, Footbridge, Large Eddy Simulation.

1. Introduction

Elevated walkways are commonly used to mitigate traffic congestion, enhance road safety, and improve pedestrian walkability in high-density cities [1]. They are designed to free pedestrians from vehicular traffic and usually have covers, which differ from viaducts. Beyond traditional traffic functions, elevated walkways are being endowed with landscaping, recreational, and commercial merit. Hong Kong is a typically densely populated metropolis. It has constructed 1,074 elevated walkways by March 2025, with more walkways in progress or planning [1]. As elevated walkways become integral to urban mobility in megacities, investigating their wind environment and thermal comfort is crucial for

enhancing pedestrian walkability and encouraging low-carbon transport modes. However, relevant research is still insufficient. Although previous studies found that perpendicular elevated walkways suppress mean flow below them [2] and the open one provides worse thermal comfort than the ground sidewalk in summer [3], these findings may not fully apply to parallel and covered elevated walkways. Therefore, this study aims to evaluate pedestrian-level wind environment and summer thermal comfort around parallel and covered elevated walkways in ideal urban building groups and explore the effects of street height-width-ratio and walkway width. Computational fluid dynamics (CFD) simulations and RayMan modeling are employed to predict the wind field and calculate *PET*.

2. Methods

2.1 CFD modeling

Following wind-tunnel models of [4], we construct ideal urban building groups that align in three rows and seven columns and are scaled down by 200. Fig. 1 shows the model schematic diagrams and dimensions. Buildings are labeled with $B_{row\text{-}column}$ for description. The approaching wind is normal to the model. No-walkway (NW) and elevated walkway (EW) models differ in whether an elevated walkway is constructed at the 5th secondary street. EW is simplified from actual prototypes, retaining primary structures like cover, floor, and supporting pillars, while ignoring elevators, stairways, railings, and handrails. Three street height-width ratios (H/W = 1, 2, 3) and three walkway widths (W_{ew}/W = 0.2, 0.4, 0.6) are designed. Only the target street canyon (marked in red) is analyzed because it is surrounded by obstacles and undergoes one of the most unfavorable wind conditions.

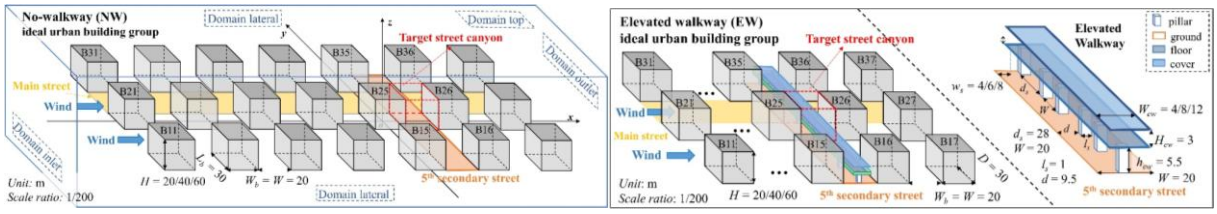

Fig. 1. Schematic diagrams and dimensions of no-walkway (NW) and elevated walkway (EW) models.

The computational domain is constructed based on the best practice guidelines [5,6], with the inlet, outlet, lateral, and top boundaries located at distances of 5*H*, 15*H*, 5*H*, and 5*H* from the model, respectively. The domain is discretized into structured hexahedral grids with a minimum grid size of 0.5 mm [7]. The velocity-inlet and pressure-outlet boundary conditions are applied at the domain inlet and outlet, respectively. Symmetry boundary condition is used for the domain top and lateral boundaries. All solid surfaces are defined as no-slip walls. The average non-dimensional distance y^+ of the first near-wall grids is below 4. The inlet profiles for wind velocity, turbulent kinetic energy, and turbulent dissipation rate are derived from wind-tunnel data [4] and [8].

CFD simulations are conducted using ANSYS Fluent 19.0 [9] on the Tianhe II supercomputer of

the National Supercomputer Center in Guangzhou, China. The equations are discretized using the finite volume scheme. The RNG k-ε model with SIMPLEC algorithm is first employed to obtain steady flow fields, providing initial conditions for further LES. Meanwhile, the second-order upwind method is used for convection and diffusion terms; the residuals are set to 10^{-4}. In LES, the Smagorinsky−Lilly model with the PISO algorithm is employed. The bounded central-differencing scheme and second-order implicit formulation are used for spatial and temporal terms. The vortex method is used to add turbulent fluctuations to the mean velocity profile [7,9]. Time step size and data sampling length are set to 0.005 s and 12 s, respectively [7]. Iterations for each time step continue until monitoring variables stabilize.

The validation case is an NW model with H = 0.125 m. Its CFD setup agrees with the above description except that the domain lateral length follows the wind-tunnel width [4]. Fig. 2 compares normalized mean wind velocity (U_{xy}/U_{ref}) at $z = 0.5H$ between wind tunnel experiments and LES. Here, U_{ref} is the reference velocity of the approaching flow at z = 0.66 m. Results show that the curves of LES results are either through or very close to the circles of wind-tunnel data. Consequently, CFD modeling of this study can accurately predict the mean flow field in an ideal urban building group.

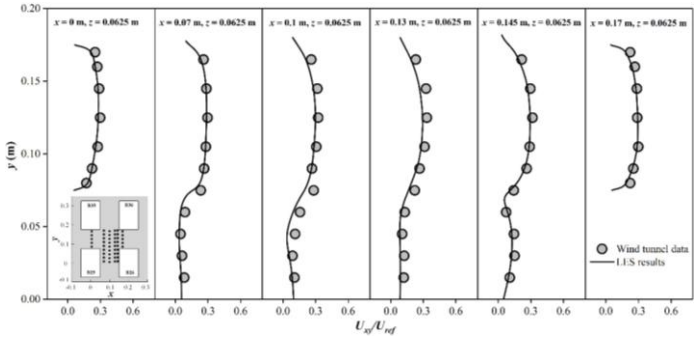

Fig. 2. Comparison of U_{xy}/U_{ref} distribution between wind-tunnel experiments and CFD simulations.

2.2 RayMan modeling

As the most widely used index in outdoor thermal comfort research, *PET* is adopted to evaluate pedestrian thermal comfort in this study. All *PET* calculations are completed in Rayman Pro 3.1 [10,11]. The simulated wind velocities ($v_{ped,\ cfd}$) are converted into in-situ velocity ($v_{ped,\ situ}$) using $v_{ped,\ cfd} \times v_{ref,\ situ}/v_{ref,\ cfd}$ before being input to Rayman Pro 3.1. Here, $v_{ref,\ situ}$ = 6.4 m/s is the mean wind velocity recorded at a remote observation site of Hong Kong, and $v_{ref,\ cfd}$ = 5.6 m/s is the mean velocity of approaching flow at the same scale height in CFD modeling. The RayMan model can simulate radiation fluxes according to the date and time, geographic location, albedo and emissivity of solid surfaces, geometrical features of buildings and vegetation, sky view factor, air temperature (T_a), relative humidity (RH), and cloud cover [10,11]. Thus, this study uses this method to compute mean radiation temperatures (T_{mrt}). Fisheye images of interest points on sidewalks and elevated walkways are obtained using the SkyHelio model [12]. The geographic location is set to 22°18'N and114°10'E (Hong Kong), and the dates are 23 August. The local time is set as 12:30 to ensure both sides of the sidewalks are directly sun-exposed. The monthly average daily maximum temperature and RH in August (T_a = 31.3 ˚C and RH = 74%) are

adopted for sidewalks [13]. Elevated walkways are assumed to have 1°C lower T_a and 3% higher *RH* than sidewalks [14]. The clothing insulation is set at 0.4 clo [15]. Pedestrians are assumed to be 25 years old, 1.75 m tall, and 70 kg in weight, walking about with a metabolic rate of 100 W [16].

3. Results and discussion

3.1 Pedestrian-level wind environment

Fig. 3 compares pedestrian-level mean wind velocity ratio (*MVR*) distributions at the target street between NW and EW cases with $W_{ew}/W = 0.4$ under different *H/W*. *MVR* is the ratio of the mean wind velocity to the inlet mean velocity at the pedestrian level ($U_{1.5m} = 2.4$ m/s). Here, the pedestrian level is 1.5 m (in full scale) above the ground. As shown in Fig. 3, EW cases have a larger low wind velocity ($MVR \leq 0.2$) region compared to NW cases with identical *H/W*, and the low wind velocity region enlarges first and then shrinks as *H/W* rises from 1 to 3. We further analyze wind conditions in the pedestrian walking zones. Thirty-one monitoring points—1.5 m above the ground or walkway floor—are set to characterize the ground sidewalk and elevated walkway. Fig. 4 shows box plots of pedestrian-level wind velocity ($v = v_{ped,\,situ}$) on the windward sidewalk (WW), leeward sidewalk (LW), and elevated walkway (EW). Regarding the mean value, WW has different *v* from LW; the ground-level *v* decreases after adding an elevated walkway in cases of *H/W* = 1, 2, and 3; EW has a higher *v* than WW and LW for five EW cases; ground-level and walkway-level *v* in EW cases show a trend of declining first and then ascending with *H/W*, while the values continuously decrease with increasing W_{ew}/W. Therefore, adding an elevated walkway in the central road generally worsens the ground pedestrian-level wind environment, but causes higher walkway-level wind velocity relative to the ground-level wind velocity.

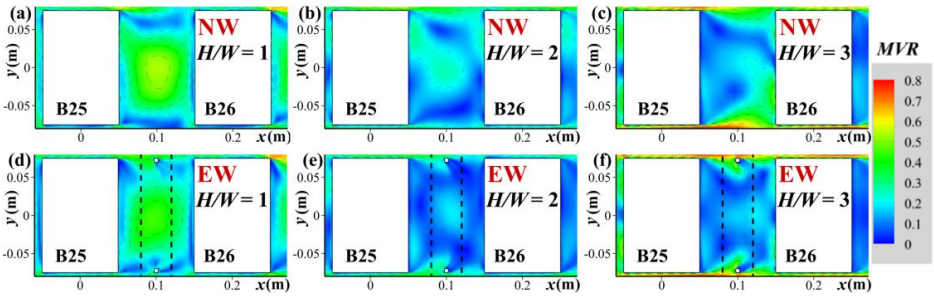

Fig. 3. Pedestrian-level *MV*R contours in NW and EW cases ($W_{ew}/W = 0.4$) with *H/W* = 1, 2, and 3.

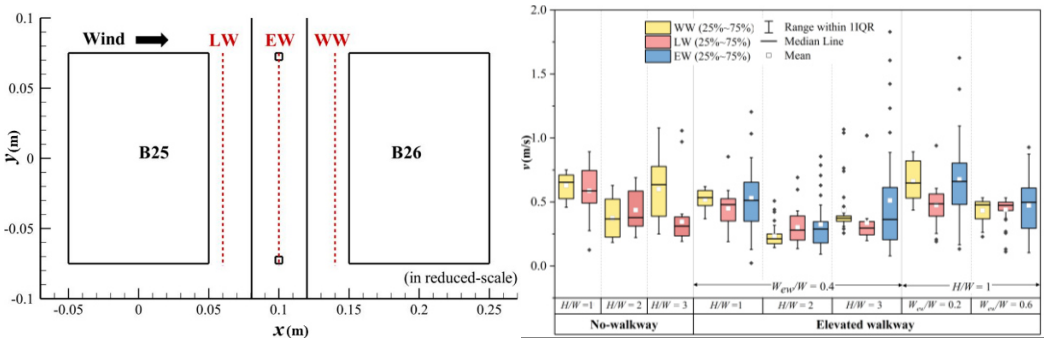

Fig. 4. Pedestrian-level wind velocity ($v = v_{ped,\ situ}$) on WW, LW, and EW in all NW and EW cases.

3.2 Pedestrian thermal comfort

Fig. 5 illustrates pedestrian-level *PET* distributions across all NW and EW cases in summer. The ground-level *PETs* are 43.0−49.6 ℃ in NW cases, indicating that pedestrians would feel hot and suffer strong heat stress [15]. In contrast, EW cases of similar *H/W* increase ground-level mean *PETs* by 0.1−1.3 ℃. For EW cases, the range of walkway-level *PETs* is 38.0−45.8 ℃, suggesting that pedestrians would feel slightly warm to warm and undergo slight to moderate heat stress [15]. Thus, the elevated walkway results in 4.4−5.8 ℃ lower mean *PETs* than the ground sidewalk. Fig. 5 also demonstrates the impacts of *H/W* and W_{ew}/W on pedestrian-level *PET*. Concerning EW cases, with *H/W* rising from 1 to 2, mean *PETs* on WW, EW, and LW increase by ~2.4 ℃, ~0.9 ℃, and ~1.3 ℃. However, mean *PET* decreases on WW and EW and varies little on LW when *H/W* varies from 2 to 3. Similar to the basic EW case of W_{ew}/W = 0.4, cases of W_{ew}/W = 0.2 and 0.6 have lower *PET* on EW than on WW and LW. Moreover, the broadening of the walkway causes increased *PET*. The maximum increase in mean *PET* occurs on WW, with an increment of ~1.7 ℃, as W_{ew}/W widens from 0.2 to 0.6. For EW, mean *PET* increases by ~0.8 ℃ when W_{ew}/W triples. In contrast, LW experiences the slightest increase in mean *PET* due to the widening walkway, as the increment is only ~0.5 ℃. Overall, although the covered elevated walkway increases ground-level *PET*, adverse to thermal comfort on ground sidewalks, it provides a lower walkway-level *PET*, effectively enhancing pedestrian thermal comfort in summer.

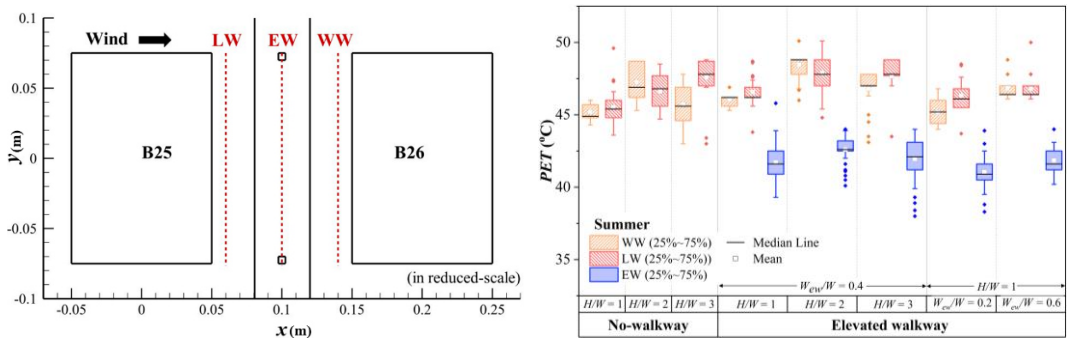

Fig. 5. Pedestrian-level *PET* distributions on WW, LW, and EW in all NW and EW cases.

4. Conclusion

This study evaluates the impacts of elevated walkway, *H/W*, and W_{ew}/W on pedestrian-level wind environment and summer thermal comfort in ideal urban building groups using LES and RayMan modeling. Through comparative analyses, it is observed that adding an elevated walkway adversely affects the ground pedestrian-level wind environment, lowering the mean wind velocity. As a result, the mean *PET* on the ground sidewalk increases slightly due to EW. Despite this, the elevated walkway provides a significantly lower walkway-level *PET*, causing improved thermal comfort and moderated heat stress in summer. Besides, both ground-level and walkway-level *PET* increase initially and

sequentially decrease when H/W rises from 1 to 3, but they positively correlate with W_{ew}/W. In contrast, ground-level and walkway-level v exhibit contrary trends to PET concerning H/W and W_{ew}/W.

5. Acknowledgements

This study was supported by the RGC Council of Hong Kong SAR, China [Grant No. T22-504/21-R] and the Postdoc Matching Fund Scheme of The Hong Kong Polytechnic University [No. 1-W34Y].

6. References

[1] Highways Department, Footbridges and subways of Hong Kong, https://www.hyd.gov.hk/en/information_corner/hyd_factsheets/doc/e_Footbridges_and_Subways.pdf.
[2] G. Duan, P. Brimblecombe, Y.L. Chu, K. Ngan, Turbulent flow and dispersion inside and around elevated walkways, *Build Environ* 173 (2020) 106711.
[3] F. Yang, F. Qian, W. Zhao, Towards a climate-responsive vertical pedestrian system: an empirical study on an elevated walkway in Shanghai, China, *Sustainability* 8 (2016) 744.
[4] B. Leitl, M. Schatzmann, Flow and dispersion in a finite array of rectangular buildings, (2010).
[5] J. Franke, Best practice guideline for the CFD simulation of flows in the urban environment, (2007).
[6] Y. Tominaga, A. Mochida, R. Yoshie, H. Kataoka, T. Nozu, M. Yoshikawa, T. Shirasawa, AIJ guidelines for practical applications of CFD to pedestrian wind environment around buildings, *J Wind Eng Ind Aerod* 96 (2008) 1749–1761.
[7] Y. Dai, C.M. Mak, Z. Ai, J. Hang, Evaluation of computational and physical parameters influencing CFD simulations of pollutant dispersion in building arrays, *Build Environ* 137 (2018) 90–107.
[8] Z.T. Ai, C.M. Mak, Large-eddy simulation of flow and dispersion around an isolated building: analysis of influencing factors, *Comput & Fluids* 118 (2015) 89–100.
[9] ANSYS Fluent 19.0, ANSYS Fluent User's Guide, Canonsburg, PA, 2018.
[10] A. Matzarakis, F. Rutz, H. Mayer, Modelling radiation fluxes in simple and complex environments – Application of the RayMan model, *Int J Biometeorol* 51 (2007) 12.
[11] A. Matzarakis, F. Rutz, H. Mayer, Modelling radiation fluxes in simple and complex environments – Basics of the RayMan model, *Int J Biometeorol* 54 (2010) 9.
[12] A. Matzarakis, O. Matuschek, Sky view factor as a parameter in applied climatology – rapid estimation by the SkyHelios model, *Meteorol Z* 20 (2011) 39–45.
[13] Hong Kong Observatory, Climatological information services: Daily exact. https://www.hko.gov.hk/en/cis/climat.htm.
[14] L. Chen, C.M. Mak, J. Hang, Y. Dai, Influence of elevated walkways on outdoor thermal comfort in hot-humid climates based on on-site measurement and CFD modeling, *Sustain Cities Soc* 100 (2024).
[15] T. Huang, J. Li, Y. Xie, J. Niu, C.M. Mak, Simultaneous environmental parameter monitoring and human subject survey regarding outdoor thermal comfort and its modelling, *Build Environ* 125 (2017) 502–514.
[16] ASHRAE Standard 55: Thermal environmental conditions for human occupancy, *ASHRAE*, 2013.